phys. stat. sol. (a) **162**, 173 (1997)

Subject classification: 61.72.Ji; 61.80.Fe; 61.72.Hh; S6

Intrinsic Defects in Cubic Silicon Carbide

H. Itoh[1]) (a), A. Kawasuso (a), T. Ohshima (a), M. Yoshikawa (a), I. Nashiyama (a), S. Tanigawa (b), S. Misawa[2]) (c), H. Okumura (c), and S. Yoshida (c)

(a) Japan Atomic Energy Research Institute, 1233 Watanuki, Takasaki, Gunma 370-12, Japan

(b) Institute of Materials Science, University of Tsukuba, 1-1-1 Tennodai, Tsukuba, Ibaraki 305, Japan

(c) Electrotechnical Laboratory, 1-1-4 Umezono, Tsukuba, Ibaraki 305, Japan

(Received January 31, 1997)

Irradiation of fast particles like 1 MeV electrons and 2 MeV protons was made for single crystalline cubic silicon carbide (3C-SiC) grown epitaxially on Si by chemical vapor deposition in order to introduce point defects in the material. Intrinsic point defects in 3C-SiC have been characterized by electron spin resonance (ESR), positron annihilation spectroscopy (PAS), Hall and photoluminescence (PL) techniques. The structure and annealing behavior of intrinsic defects, e.g. monovacancies at silicon and carbon sublattice sites, are described based on the results obtained by ESR and PAS. The contributions of such point defects to electrical and optical properties of 3C-SiC are discussed using the Hall and PL results, with a brief review of published work.

1. Introduction

Silicon carbide (SiC) has high temperature stability, high thermal conductivity, outstanding semiconducting properties at high temperatures, and excellent chemical and radiation resistance. From these properties, SiC is considered as a promising material for high-power, high-frequency, high-temperature, and radiation-resistant devices [1]. Moreover, this unique combination of properties makes this material suitable for very high-speed microprocessors. Especially, cubic SiC (3C-SiC), which has zinc-blende structure, exhibits a small band gap ($E_g \approx 2.3$ eV at 300 K) and quite good electrical properties such as high electron mobility and saturation drift velocity [2, 3] in comparison with the other polytypes. Thus, 3C-SiC is expected to be the most desirable material for the application to SiC integrated circuits. In addition, since 3C-SiC has a simple cubic structure different from the other polytypes, it is suitable to investigate the nature of intrinsic defects in SiC. From this reason, a lot of theoretical researches on defects have dealt with this material [4 to 8]. On the other hand, little was known about point defects in 3C-SiC until the early 1980s because high-quality 3C-SiC single crystals had been hardly obtained. This situation was changed drastically due to the success in heteroepitaxial growth of 3C-SiC on Si substrates [9 to 12] by chemical vapor deposition (CVD). Adopt-

[1]) Present address: University of Erlangen-Nürnberg, Institute of Applied Physics, Staudtstraße 7, D-91058 Erlangen, Germany.

[2]) Present address: ULVAC Corp., 5-9-7 Tohkohdai, Tsukuba, Ibaraki 305-26, Japan.

ing this technique, single crystalline 3C-SiC in which impurities are well controlled has been obtained reproducibly. This improvement in the crystal quality stimulated experimental investigastions as well as theoretical studies of defects in 3C-SiC, and thus considerable results have been accumulated up to now, see e.g. a recent review work of Schneider and Maier [13]. Nevertheless, the structure, electronic levels, and annealing behavior of intrinsic defects in 3C-SiC have not yet been fully understood.

In the early state of defect studies in 3C-SiC, Balona and Loubser [14] performed electron spin resonance (ESR) measurements of electron and neutron irradiated 3C-SiC, and found an F signal which was supposed to be responsible for carbon divacancies. Geiczy et al. [15, 16] reported defect related cathodoluminescence (CL) lines A_0, B_0, C_0 and D_0 in electron irradiated 3C-SiC. The C_0 CL line was speculated to be related to defects at carbon sites and the others were supposed to be caused by defects at silicon sites. Photoluminescence (PL) measurements by Choyke and Patrick [17 to 19] showed the formation of D_1 and D_2 defects in 3C-SiC by ion irradiation and subsequent annealing. They proposed that the D_1 and D_2 PL lines arose from divacancies and carbon di-interstitials, respectively. After the success in the CVD growth of 3C-SiC, many experimental attempts to reveal the structure and electronic levels of point defects have been made using CVD-grown epilayers. Nagesh et al. [20, 21] performed deep-level transient spectroscopy (DLTS) and resistivity measurements of neutron irradiated 3C-SiC epilayers. As a result, they found a point defect related electron trap E2 ($E_c - 0.49$ eV), and hole traps H1 ($E_v + 0.18$ eV), H2 ($E_v + 0.24$ eV), and H3 ($E_v + 0.514$ eV). Most electronic levels of defects produced by neutron irradiation were, however, reported to be confined to the middle third of the band gap. Freitas et al. [22] reported the D_1 and D_2 PL lines in ion implanted 3C-SiC epilayers, and presented that their intensities increased with annealing temperature up to 1600 °C. Nashiyama et al. [23] investigated the displacements of Si and C atoms in proton irradiated 3C-SiC by using ^{12}C (d, p) ^{13}C nuclear reaction and deuteron Rutherford backscattering technique. Their results indicated that C interstitials were located mostly at tetrahedral-like interstitial sites. Itoh et al. [24 tob 28] made ESR measurements of 3C-SiC epilayers irradiated with electrons and protons, and found ESR signals T1, T5, T6, and T7 ascribed to intrinsic point defects. They identified the T1 signal to arise from a negatively charged silicon vacancy (V_{Si}^-). Positron annihilation spectroscopy (PAS) was also applied to the study of point defects in electron irradiated 3C-SiC epilayers [26, 29, 30], and the results supported the formation of V_{Si}^-. The T5 signal observed in p-type 3C-SiC was found to be attributed to a positively charged carbon vacancy (V_C^+) [27]. The T6 and T7 centers were proposed to be some forms of vacancy–interstitial pairs [28]. It was shown from PL measurements of electron irradiated 3C-SiC that the irradiation induced 1.913 eV PL line is caused by V_{Si} [31]. Son et al. [32] performed PL and optically detected magnetic resonance (ODMR) measurements of electron irradiated 3C-SiC epilayers. They found an ODMR center labeled L2 giving rise to a PL emission at 1.121 eV, and explained that this defect was related to V_{Si}.

In this paper, our recent researches on intrinsic point defects in 3C-SiC are described with a brief review of published work. We deal with intrinsic point defects introduced in CVD-grown 3C-SiC epilayers by irradiation of fast particles like 1 MeV electrons and 2 MeV protons. Since ESR and PAS are regarded as quite useful techniques for a microscopic understanding of point defects in semiconductors, concerning defect identification by ESR, see e.g. [33], regarding characterization of defects by PAS, see e.g. [34], these

methods were used to investigate the structure of defects and their annealing behavior. After a brief report of experimental procedures in Section 2, identification of the defect structure based on the ESR results is described in Section 3.1. Characterization of vacancy-type defects using the results of Doppler broadening and positron lifetime measurements are stated in Section 3.2. In Section 3.3, we show the annealing behavior of point defects. The effects of intrinsic point defects on electrical and optical properties of 3C-SiC are discussed in Sections 4.1 and 4.2 in connection with the Hall and PL results. A brief discussion on electronic levels of intrinsic defects is given in Section 4.3. A summary will be given in the final section.

2. Experimental Procedures

Single crystalline 3C-SiC films with the thickness of $\approx 30\,\mu m$ were grown epitaxially at 1410 °C on Si(100) substrates by CVD. In the growth, SiH_4 and C_3H_8 were used as source gases in a flow of pure H_2 carrier gas. Details of the growth procedure have been described in [10]. The unintentionally doped films exhibited n-type electrical conduction with the carrier concentration of $\approx 1 \times 10^{16}/cm^3$ and the Hall mobility of $\approx 500\,cm^2/Vs$ at room temperature (RT). For the growth of p-type 3C-SiC films, Al impurities were doped by a mixture of $Al(CH_3)_3$ in the source gases. The as-grown p-type films showed a hole concentration of $\approx 1 \times 10^{17}/cm^3$ at RT. After the growth, the Si substrates were etched off with an $HF-HNO_3$ solution for ESR and position lifetime measurements. These epilayers were irradiated with 1 MeV electrons or 2 MeV protons to introduce point defects. Electron irradiation was made in an Ar atmosphere in the fluence range up to $1 \times 10^{19}\,e/cm^2$ at the fluence rate $\approx 3 \times 10^{13}\,e/cm^2\,s$. The samples were mounted on a water-cooled holder so as to avoid beam heating, and their temperature was kept below 50 °C during electron irradiation. Protons were irradiated to 3C-SiC samples at fluences up to $6 \times 10^{16}\,H^+/cm^2$, where the fluence rate was $\approx 3 \times 10^{12}\,H^+/cm^2\,s$. In proton irradiation, the samples were placed on a Cu heat sink so that their temperature was kept below 50 °C. Isochronal annealing of irradiated samples was performed for 5 min in a dry, pure Ar atmosphere.

ESR measurements of 3C-SiC films were made at temperatures from 4 K to RT with an X-band (9 GHz) microwave incident on a TE_{011} cylindrical cavity. The spin number of paramagnetic defects was determined using the spin standards diphenyl-picryl hydrazyl (DPPH) and Mn^{2+} in MgO. PL measurements were performed for 3C-SiC/Si samples in the temperature range from 4 to 200 K by using an Ar-ion laser with lines at 351.1 and 363.8 nm. The excitation laser light was focused on the sample surface to a spot with a $\approx 200\,\mu m$ diameter, and its power was approximately $30\,W/cm^2$. The penetration depth of the laser light is estimated to be 3 to 5 μm, so that the obtained PL spectra are due to photon emission from the 3C-SiC films only. In the Doppler broadening experiments, positrons emitted from a ^{22}Na source were moderated with W foils and subsequently accelerated with a variable electric field. Positrons with an energy up to 30 keV were implanted into 3C-SiC/Si samples at RT. The penetration depth of positrons at 30 keV is $\approx 3\,\mu m$. The energy spectrum of annihilation γ-rays was measured with a high-purity Ge detector. The Doppler broadened energy spectrum was characterized by the lineshape parameter S, which was defined as the integral of γ-ray intensity in the central energy region (511 ± 0.5) keV divided by the total intensity. In the positron lifetime measurements, a ^{22}Na source was sandwiched by two 3C-SiC film samples.

On both sides of the set of samples, p-type 6H-SiC wafers with the thickness of ≈300 μm were placed so as to avoid a superposition of unknown lifetime signals caused by annihilation of positrons traveling through 3C-SiC films. Positron lifetime was measured at RT using a conventional fast–fast spectrometer with a time resolution ≈200 ps at RT. The lifetime spectrum obtained was analyzed using the computer code PATFIT-88 [35]. Since the average lifetimes of positrons in as-grown and electron irradiated n-type 3C-SiC samples were longer than that for p-type 6H-SiC, the obtained lifetimes are attributable to positron annihilation in 3C-SiC.

3. Defect Structure and Annealing Behavior

3.1 Paramagnetic point defects: ESR centers

3.1.1 Silicon vacancy

Fig. 1 shows a typical ESR spectrum at 10 K for n-type 3C-SiC irradiated with protons when the magnetic field was applied parallel to the ⟨100⟩ axis (**H** ∥ ⟨100⟩). In this spectrum, an ESR signal labeled T1 [24 to 26] is clearly observed. The T1 signal was also observed in n-type and p-type 3C-SiC samples irradiated with 1 MeV electrons, reactor neutrons, or high-energy heavy ions like 120 MeV Ne^{6+}. This symmetric signal consists of fifteen ESR lines, i.e., the central five lines equally spaced at ≈1.5 G intervals and the satellite five lines equally spaced at ≈1.5 G, which are disposed on both sides of the

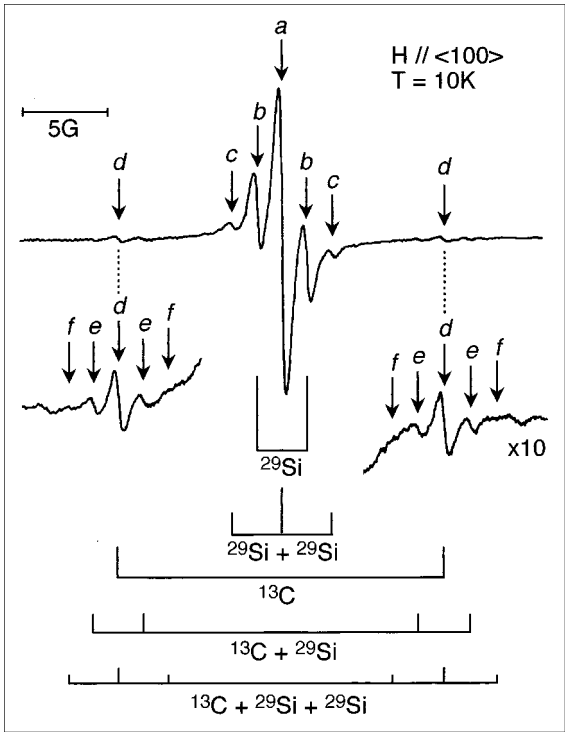

Fig. 1. ESR spectrum at 10 K for n-type 3C-SiC irradiated with 2 MeV protons at 1×10^{16} H^+/cm^2. The magnetic field was applied parallel to the ⟨100⟩ axis. Fifteen lines of the T1 signal are indicated by the arrows a, b, c, d, e, and f. Hyperfine interactions with ^{13}C and ^{29}Si resulting in each ESR line are also represented

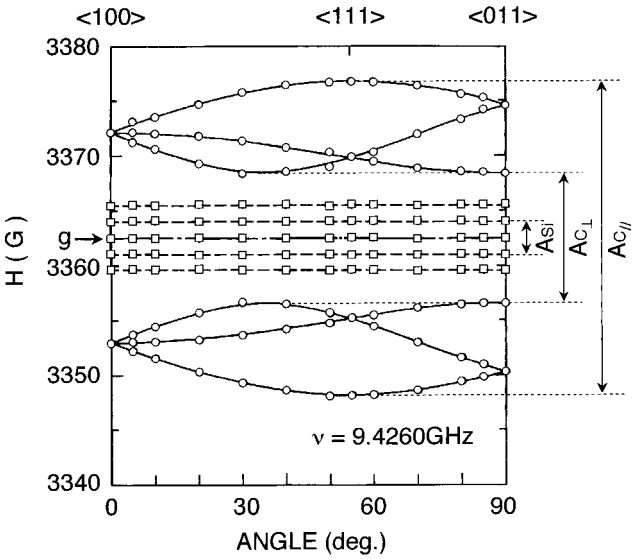

Fig. 2. Angular dependence of the T1 signal. The magnetic field was rotated in the {011} plane. The abscissa indicates the angle between the magnetic field and the ⟨100⟩ axis. The squares and circles represent the positions of the central five lines (a, b, c) and the satellite lines d, respectively. The solid curves correspond to the calculated angular dependence of the satellite lines d, which result from hyperfine interactions with ^{13}C, by using the spin Hamiltonian eq. (1) in text and the ESR parameters listed in Table 1

central five lines, in $\mathbf{H} \parallel \langle 100 \rangle$. The T1 signal was observed in a wide temperature range between 4 K and RT. Here, the fifteen ESR lines are labeled a, b, c, d, e, and f, as represented in Fig. 1. For the central five lines, the intensity ratios of the sidelines b and c to the central line a were 0.266 ± 0.02 and 0.035 ± 0.01, respectively. Almost the same intensity ratios were obtained for the satellite five lines. The intensity ratio of the line d to the central line a was 0.018 ± 0.005. The angular dependence of the T1 signal is shown in Fig. 2, where the magnetic field was rotated in the {011} plane. The positions of the five satellite lines were found to depend on the angle between the magnetic field and the ⟨100⟩ axis, while no significant change was observed in the positions of the central five lines.

The total intensity of the satellite lines d relative to the central line a is approximately four times as large as the natural abundance of ^{13}C (1.1%), which has a nuclear spin $I_C = 1/2$. The total intensity of the lines b relative to the central line a is about twelve times as large as the natural abundance of ^{29}Si (4.7%) which also has a nuclear spin $I_{Si} = 1/2$. These facts suggest strongly that the T1 signal is caused by the Zeeman interaction and simultaneous hyperfine (hf) interactions of paramagnetic electrons with ^{13}C at four carbon sites and ^{29}Si at twelve silicon sites. Here, the probability that one ^{13}C atom exists at any of four carbon sites is obtained from the natural abundance of ^{13}C to be 0.043. The probabilities that one and two ^{29}Si atoms exist at any of twelve silicon sites are 0.331 and 0.089, respectively. Since the probabilities that two or more ^{13}C exist and that three or more ^{29}Si exist are very low, these hf interactions are negligible. Thus, the T1 signal exhibiting the angular dependence shown in Fig. 2 can be repre-

sented by the spin Hamiltonian.

$$\mathscr{H} = \beta \mathbf{SgH} + \mathbf{SA}_{\mathrm{C}}\mathbf{I}_{\mathrm{C}} + \sum_{j=1}^{2} \mathbf{SA}_{\mathrm{Si}}\mathbf{I}_{\mathrm{Si}}\,, \tag{1}$$

with an effective spin $S = 3/2$. Determination of the spin state of the T1 center is described later. In eq. (1), the first term indicates the Zeeman interaction which gives the position of the central line a. The second term represents hf interactions with ^{13}C giving the positions of the ESR lines d, and the third term hf interactions with ^{29}Si showing the positions of the lines b and c (Fig. 1).

Table 1

ESR centers originated from intrinsic point defects in 3C-SiC. ESR parameters (S, $\mathbf{g}$, $\mathbf{A}$, and $\mathbf{D}$) and wave function coefficients (η^2, α^2, and β^2), which were calculated from the obtained $\mathbf{A}$ tensors by using an LCAO method, are indicated for each ESR center. The conduction type of 3C-SiC (n or p) and temperature range (T_{obs}), in which each ESR signal was observed, are also presented. Particles e, H^+, n, and ions correspond to 1 MeV electrons, 2 MeV protons, reactor neutrons, and high-energy heavy ions like 120 MeV Ne^{6+}, respectively. K and T_{ann} represent the introduction rate in 1 MeV electron irradiation and the annealing stages, respectively, for every ESR center

ESR center	T1	T5	T6	T7
cond. type	n, p	p	p	p
irradiation particle	e, H^+, n, ions	e, H^+	e	e
T_{obs} (K)	4 to 300 (full range)	$\leq$100	4 to 300 (full range)	$\leq$150
S	3/2	1/2	1	1
g	$g = 2.0029$	$g_1 = 2.0020$ $g_2 = 2.0007$ $g_3 = 1.9951$	$g \approx 2.003$	$g \approx 2.01$
A (cm^{-1})	$A_{\mathrm{C}_\parallel} = 2.67 \times 10^{-3}$ $A_{\mathrm{C}_\perp} = 1.10 \times 10^{-3}$ ($A_{\mathrm{C}} \parallel \langle 111 \rangle$) $A_{\mathrm{Si}} = -2.73 \times 10^{-4}$	$A_{\mathrm{Si}_\parallel} = -1.89 \times 10^{-3}$ $A_{\mathrm{Si}_\perp} = -1.38 \times 10^{-3}$ ($A_{\mathrm{Si}} \parallel \langle 111 \rangle$)	–	–
D (cm^{-1})	–	–	$\lvert D\rvert = 1.2 \times 10^{-2}$ ($D \parallel \langle 111 \rangle$)	$\lvert D\rvert = 5.2 \times 10^{-2}$ ($D \parallel \langle 111 \rangle$)
wave function coefficient	nearest C site $\eta^2 = 0.19$ $\alpha^2 = 0.08, \beta^2 = 0.92$ 2nd-nearest Si site $\eta^2 = 0.01$ ($\alpha^2 = 0.25, \beta^2 = 0.75$)	nearest Si site $\eta^2 = 0.073$ $\alpha^2 = 0.19, \beta^2 = 0.81$	–	–
K (cm^{-1})	1.7×10^{-2} (n-type)	3.3×10^{-3}	3.4×10^{-1}	1.9×10^{-2}
T_{ann} (°C)	150, 350, 750	150	300	300
structure	V_{Si}^- (T_d symmetry)	V_{C}^+ (D_2 symmetry)	V–I $r = 6.1$ Å	V–I $r = 3.8$ Å

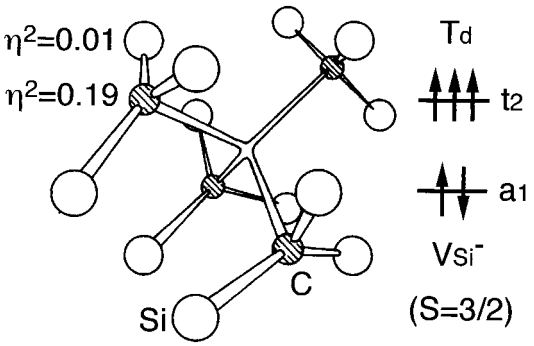

Fig. 3. Structural model of the T1 center: a negatively charged vacancy at a silicon sublattice site V_{Si}^{-}. Electronic states are also represented for V_{Si}^{-} (spin state $S = 3/2$) with T_d symmetry. The number denoted next C or Si atom indicates the existence probability (η^2) of paramagnetic electrons at each site

The intensity ratio of the ESR line d to the line a was calculated by using eq. (1) to be 0.022. The intensity ratios of the lines b and c to the central line a were also obtained to be 0.265 and 0.036, respectively. These values agree well with those obtained experimentally. The angular dependence of the central line a indicates that the T1 signal has an isotropic g-value of 2.0029 ± 0.0001. The anisotropy of the satellite lines d is in excellent agreement with that calculated from the $\langle 111 \rangle$ axially symmetric hf tensor of $|A_{C_\parallel}|/g\beta = 28.6$ G and $|A_{C_\perp}|/g\beta = 11.8$ G, as shown in Fig. 2. Taking account of the positive sign of the carbon nuclear moment, $A_{C_\parallel}$ and $A_{C_\perp}$ are estimated to be 2.67×10^{-3} and $1.10 \times 10^{-3}\,\mathrm{cm}^{-1}$, respectively. The angular dependence of the ESR lines b represents the nearly isotropic hf tensor $|A_{Si}|/g\beta = 2.94$ G. Considering the negative sign of the silicon nuclear moment, $A_{Si} = -2.73 \times 10^{-4}\,\mathrm{cm}^{-1}$ is obtained. ESR parameters obtained for the T1 signal are listed in Table 1. All the results show that the T1 signal originates from the Zeeman interaction and the hf interactions with ^{13}C and ^{29}Si nuclear spins, which are shown in Fig. 1: The most intense central line a is mainly caused by the Zeeman interaction. The sidelines b and c are ascribed to the hf interactions with one ^{29}Si and two ^{29}Si nuclear spins, respectively. The satellite lines d result mainly from the hf interaction with ^{13}C. The lines e and f are due to the simultaneous hf interactions with ^{13}C and ^{29}Si nuclear spins.

Fig. 3 shows the structural model of the T1 center, i.e. a monovacancy at a silicon sublattice site V_{Si}, which is surrounded by four nearest-neighbor carbon atoms and twelve second-nearest-neighbor silicon atoms. The isotropic g-tensor obtained for the T1 signal leads to T_d symmetry of this defect. The axially symmetric hf tensor along the $\langle 111 \rangle$ axis for the hf interaction with ^{13}C supports our model that four nearest-neighbor carbon atoms are located equivalently in the $\langle 111 \rangle$ direction from the vacancy site. In contrast to the hf interaction with ^{13}C, that with ^{29}Si at the second-nearest-neighbor sites is so weak that it represents a quite small anisotropy, which accounts for the result that the central five lines were nearly isotropic.

The introduction rate of the T1 center for 1 MeV electron irradiation was obtained to be $1.7 \times 10^{-2}\,\mathrm{cm}^{-1}$ in n-type 3C-SiC [25]. This value is very close to the carrier removal rate $1.4 \times 10^{-2}\,\mathrm{cm}^{-1}$ [36] obtained for 1 MeV electron irradiation into n-type epilayers. Moreover, it was found from isochromal annealing that the electron concentration recovered at almost the same temperatures as the T1 center was annealed [36]. These results indicate that the T1 center captures an electron from the conduction band, i.e., V_{Si} is charged negatively. Thus, the spin state of the T1 center is considered as $S = 3/2$: Two electrons occupy an a_1 state and the other three electrons a t_2 state, as represented in

Fig. 3. Generally we have to take a fine interaction term **SDS** into the spin Hamiltonian in the case of $S \geq 1$. However, all the components of **D** become zero when the defect has T_d symmetry. Therefore, even for $S = 3/2$ we can ignore the fine interaction term in the spin Hamiltonian (eq. (1)) used for the analysis of the T1 signal.

One may propose the possibilities that the T1 signal arises from an antisite defect at a silicon site C_{Si} and that some impurities are incorporated in the T1 structure. It was reported that V_{Si} has a gap state but C_{Si} has no gap state in 3C-SiC [4 to 8]. Furthermore, no ESR line was observed for the hf interaction with the antisite ^{13}C. Thus, the first possibility can be ruled out. The formation of V_{Si} was also shown from the PAS measurements of electron irradiated samples, which is described in Section 3.2. As for impurities, it is probable that N and H impurities are incorporated in as-grown 3C-SiC films. If these impurities are involved in the defect, electron spins should interact with ^{14}N (nuclear spin $I_N = 1$, natural abundance 99.64%) and with ^{1}H (nuclear spin $I_H = 1/2$, natural abundance 99.98%), giving rise to the hf splitting of an ESR line in three and two lines, respectively. However, ESR lines of the T1 signal cannot be explained by the hf interactions with ^{14}N and ^{1}H, leading to the fact that these impurities do not exist in the vicinity of the defect. In addition, T_d symmetry of the T1 center suggests strongly that no impurity is included in the defect structure. From these facts, the second possibility is also denied. Consequently, we conclude that the T1 center is a negatively charged silicon vacancy (V_{Si}^-). Negatively charged vacancies with $S = 3/2$, which show T_d symmetry, were also reported for diamond [37].

Here we consider the distribution of paramagnetic electrons on the nearest-neighbor carbons in the T1 center. The electronic wave function Ψ can be constructed with a linear combination of atomic orbitals (LCAO) centered on the nearest-neighbor carbon sites. When we approximate the carbon orbital at each site k as hybrid C 2s 2p orbitals, Ψ is described as

$$\Psi = \sum_k \eta_k(\alpha_k(\varphi_{2s})_k + \beta_k(\varphi_{2p})_k)\,. \tag{2}$$

For carbon atoms adjacent to the vacancy, the 2p orbital is thought to be directed to the center of the vacancy along the $\langle 111 \rangle$ direction from the carbon sites. Then, the axially symmetric hf tensor can be represented as

$$\begin{aligned} A_{\parallel} &= A_s + 2A_p\,, \\ A_{\perp} &= A_s - A_p\,. \end{aligned} \tag{3}$$

Here, the isotropic term A_s results from the Fermi contact interaction and the anisotropic term A_p arises from the dipole–dipole interaction averaged over the electronic wave function. From the values of $A_{\parallel}$ and $A_{\perp}$ for the hf interaction with ^{13}C, we obtain $A_s = 1.62 \times 10^{-3}\,\mathrm{cm}^{-1}$ and $A_p = 5.23 \times 10^{-4}\,\mathrm{cm}^{-1}$. Using the values of A_s and A_p calculated for 100% localization of an unpaired electron in C 2s and 2p orbitals [38], η^2, α^2, and β^2 are estimated to be 0.19, 0.08, and 0.92, respectively, and they are listed in Table 1. This means that 76% of the wave function is located on the nearest-neighbor carbon orbitals. A strong p-character ($\beta^2/\alpha^2 = 11.5$) suggests strongly that the four carbon atoms are rearranged equivalently along the $\langle 111 \rangle$ direction with keeping the T_d symmetry.

The LCAO treatment can be extended to the analysis of the electron distribution on the second-nearest-neighbor silicon atoms. Here we assume sp^3 admixture orbitals

($\alpha^2 = 0.25$ and $\beta^2 = 0.75$) for the second-nearest-neighbor silicon atoms. From the experimentally obtained value $A_{Si} = -2.73 \times 10^{-4}\,cm^{-1}$ and the calculated values A_s and A_p for 100% electron localization in Si 3s and 3p orbitals [38], η^2 is estimated to be 0.01. This result represents that approximately 12% of the wave function is located on the twelve second-nearest-neighbor silicon atoms. Most of the residual 12% is probably spread out over more distant sites. The large value of η^2 for the nearest-neighbor carbons implies that the T1 center forms a deep level in the 3C-SiC band gap, which is consistent with the result that the T1 signal was observable at RT. Discussion of this defect level will be shown in Section 4.3.

3.1.2 Carbon vacancy

In Al-doped p-type samples, additional ESR signals were observed after electron or proton irradiation. Fig. 4 shows a typical ESR spectrum at 10 K for p-type 3C-SiC irradiated with protons when $\mathbf{H} \parallel \langle 111 \rangle$. In this spectrum, an ESR signal labeled T5 [27] as well as the T1 signal can be seen. The T5 signal was observed at temperatures below ≈100 K in p-type 3C-SiC samples irradiated with protons and electrons. On the other hand, this signal was not observed in n-type samples. The T5 signal was found to consist of main three ESR lines and weak ESR lines disposed on either side of the main lines. The intensity ratio of all weak satellite lines to the main lines was 0.185 ± 0.02, which is approximately four times as large as the ^{29}Si abundance. This fact suggests that the satellite lines result from the hf interaction with ^{29}Si at four silicon sites. Here, the probability that one ^{29}Si exists at any of the four silicon sites is derived to be 0.163. Since the probability that two or more ^{29}Si exist is less than 0.012, the hf interactions with such multiple nuclear spins can be neglected. The angular dependence of the T5 signal is shown in Fig. 5, where the magnetic field was rotated in the {011} plane. The T5 signal with an anisotropy can be represented by the spin Hamiltonian

$$\mathcal{H} = \beta \mathbf{S} \mathbf{g} \mathbf{H} + \mathbf{S} \mathbf{A}_{Si} \mathbf{I}_{Si}\,, \tag{4}$$

with an effective electron spin $S = 1/2$. The first Zeeman interaction term gives the positions of the main three lines. The second term indicates the hf interactions of an electron spin with a nuclear spin $I_{Si} = 1/2$ of ^{29}Si, which give the positions of the weak

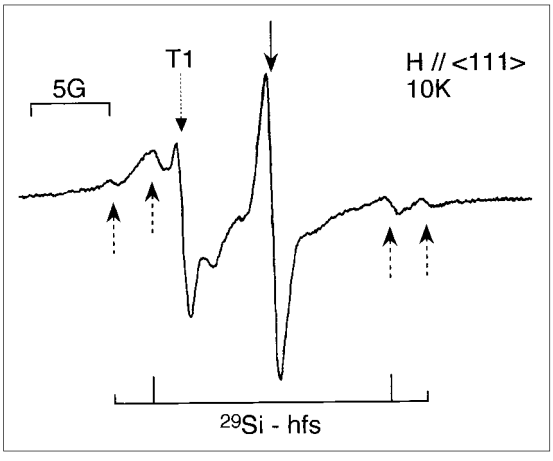

Fig. 4. ESR spectrum at 10 K for p-type 3C-SiC irradiated with 2 MeV protons at $1 \times 10^{15}\,H^+/cm^2$ when the magnetic field was applied parallel to the ⟨111⟩ axis. ESR lines arising from the Zeeman and ^{29}Si hyperfine interactions in the T5 signal are indicated by the solid and broken-line arrows, respectively. The dotted-line arrow represents the position of the T1 signal

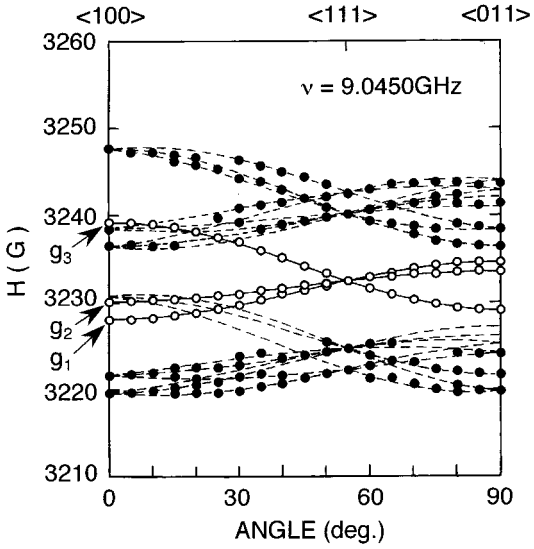

Fig. 5. Angular dependence of the T5 signal. The magnetic field was rotated in the {011} plane. The abscissa indicates the angle between the magnetic field and the ⟨100⟩ axis. The open and closed circles indicate the positions of the main and weak satellite lines, respectively. The solid and broken curves represent the calculated angular dependences of the main and satellite ESR lines, respectively, by using the spin Hamiltonian eq. (4) in text and the ESR parameters listed in Table 1. The arrows indicate the positions giving the principal values of g tensor, g_1, g_2, and g_3

satellite lines (Fig. 4). By using eq. (4), the relative intensity of all the satellite lines to the main lines is estimated to be 0.194. This value agrees well with the intensity ratio obtained experimentally. The principal values of the g-tensor are obtained from the angular dependence of the main three lines to be $g_1 = 2.0020 \pm 0.0001$, $g_2 = 2.0007 \pm 0.0001$, and $g_3 = 1.9951 \pm 0.0001$, which are directed along the ⟨100⟩ axes. The anisotropy of the satellite lines is well represented by an axially symmetric hf tensor along the ⟨111⟩ axis, i.e., $A_{\mathrm{Si}} = -1.89 \times 10^{-3}\,\mathrm{cm}^{-1}$ ($|A_{\mathrm{Si}_\parallel}|/g\beta = 20.3\,\mathrm{G}$) and $A_{\mathrm{Si}_\perp} = -1.38 \times 10^{-3}\,\mathrm{cm}^{-1}$ ($|A_{\mathrm{Si}_\perp}|/g\beta = 14.8\,\mathrm{G}$), which are shown in Table 1.

Fig. 6 shows the structural model of the T5 center, i.e., an isolated vacancy at a carbon sublattice site V_C. The hf structure (hfs) with ^{29}Si at the four silicon sites indicates a fourfold coordination of silicon atoms around the defect, which is consistent with this model. In contrast to the T1 signal, the hf interactions with ^{13}C at the second-nearest-

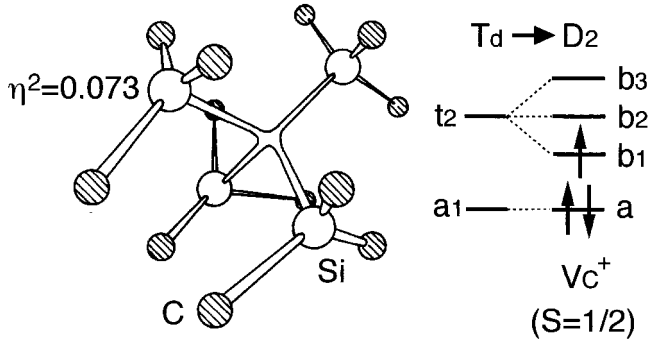

Fig. 6. Structural model of the T5 center: a positively charged carbon vacancy V_C^+. Electronic states are also shown for V_C^+ with $S = 1/2$. D_2 symmetry of this defect is caused mainly by a Jahn-Teller distortion. The number next Si atom means the existence probability of a paramagnetic electron at the nearest-neighbor site

neighbor carbon sites are too weak to split the main lines. The principal values and directions of the g-tensor for the T5 center show D_2 symmetry of this defect, which is thought to be mainly due to a Jahn-Teller distortion. Moreover, no fine structure observed for the T5 signal indicating D_2 symmetry suggests strongly that the spin state of the T5 center is 1/2. It shows that the T5 center is a positively charged carbon vacancy V_C^+ (Fig. 6). In this case, two electrons occupy an a state and another electron occupies a b_1 state, which causes the T5 signal.

Theoretical investigations showed that V_C has a gap state but an antisite at a carbon site Si_C has no gap state in 3C-SiC [4 to 8]. In addition, no hfs due to antisite ^{29}Si was observed in the ESR spectra of irradiated p-type samples. This supports our model that the T5 signal does not arise from Si_C but results from V_C. If Al impurities, which were doped in p-type samples, are incorporated in the T5 structure, an ESR line should be split into six lines due to hf interactions with ^{27}Al (nuclear spin $I_{Al} = 5/2$, natural abundance 100%). However, the main three lines and satellite lines in the T5 signal cannot be represented by the hf interactions with ^{27}Al. Thus, it can be concluded that Al impurities are not located in the vicinity of V_C. The introduction rate of the T5 center was obtained to be $3.3 \times 10^{-3}\,cm^{-1}$ for 1 MeV electron irradiation. This value is lower than that for the T1 center ($1.7 \times 10^{-2}\,cm^{-1}$), which is probably related to a small cross section for the displacement of carbon atoms compared with that for silicon atoms and partial annealing of the T5 center during electron irradiation. Annealing of ESR centers is described in Section 3.3. The experimental fact that the T5 signal was not observed in n-type samples can be interpreted by the difference in the charge state of V_C: The charge state of V_C is probably neutral in n-type 3C-SiC and neutral V_C, i.e., V_C^0 with an effective spin $S = 0$ is undetectable by ESR.

The distribution of a paramagnetic electron on the nearest-neighbor silicon sites in the T5 center can be estimated by a simple LCAO method as used for the analysis of the T1 center. In this case, we approximate the silicon orbital ψ_k at each site k as hybrid Si 3s 3p orbitals: $\psi_k = \alpha_k(\varphi_{3s})_k + \beta_k(\varphi_{3p})_k$. Substituting the experimentally obtained hf parameters $A_{Si_\parallel} = -1.89 \times 10^{-3}\,cm^{-1}$ and $A_{Si_\perp} = -1.38 \times 10^{-3}\,cm^{-1}$ for eq. (3), we can obtain $A_s = -1.55 \times 10^{-3}\,cm^{-1}$ and $A_p = -1.71 \times 10^{-4}\,cm^{-1}$. Taking account of the values A_s and A_p for 100% localization of electronic wave function in Si 3s and 3p orbitals [38], η^2, α^2, and β^2 are estimated to be 0.073, 0.19, and 0.81, respectively (Table 1). Thus, approximately 29% of the total electronic wave function is thought to be located on the nearest-neighbor silicon atoms adjacent to the vacancy. The dangling orbitals are also shown to contain 19% 3s and 81% 3p character. The residual 71% of the wave function is spread out over the second-nearest-neighbor or more distant sites.

3.1.3 Other ESR centers

Fig. 7 shows ESR spectra at 20 K for p-type 3C-SiC irradiated with electrons when $\mathbf{H} \parallel \langle 011 \rangle$. In addition to the T1 and T5 signals, two ESR signals labeled T6 and T7 [28] are observed. The T6 signal was observed in the temperature range between 4 K and RT. On the other hand, the T7 signal was observable below ≈150 K. The angular dependence of both signals is shown in Fig. 8. Both signals can be represented by the spin Hamiltonian

$$\mathscr{H} = \beta \mathbf{S} g \mathbf{H} + \mathbf{S} D \mathbf{S}\,, \tag{5}$$

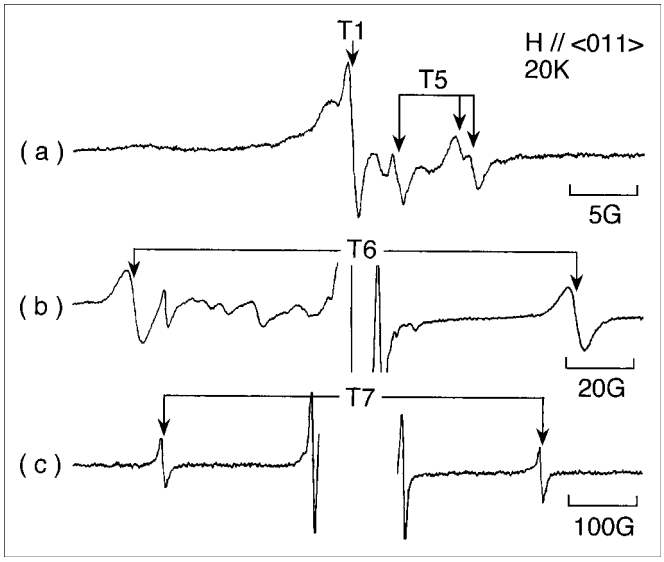

Fig. 7. ESR spectra at 20 K for p-type 3C-SiC irradiated with 1 MeV electrons at 1.8×10^{18} e/cm^2 when the magnetic field was applied parallel to the $\langle 011 \rangle$ axis. Sweep ranges of the magnetic field are approximately (a) 40, (b) 160, and (c) 800 G. ESR lines of the T6 and T7 signals are shown by arrows in (b) and (c), respectively

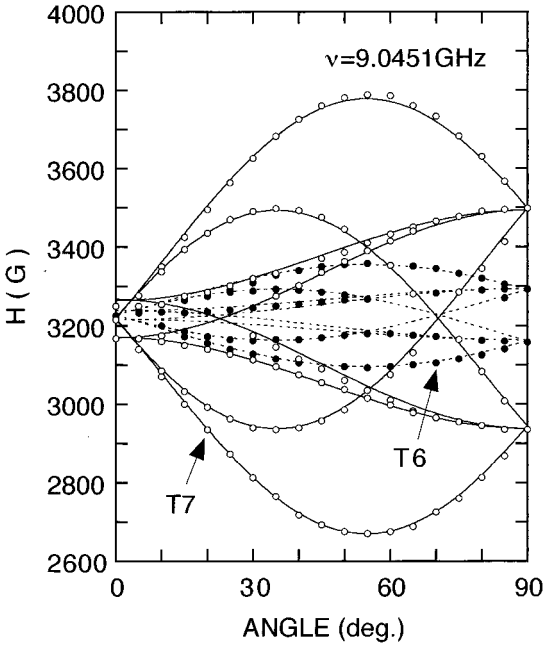

Fig. 8. Angular dependence of the T6 and T7 signals. The closed and open circles represent the positions of the T6 and T7 ESR lines, respectively. The sample was rotated around the [01$\bar{1}$] axis perpendicular to the magnetic field, but the rotation axis was inclined by 3.5° toward the [100] axis. The dotted and solid curves indicate the angular dependences of the T6 and T7 signals, respectively, calculated using the spin Hamiltonian eq. (5) in text and the ESR parameters listed in Table 1

with an effective spin $S = 1$. The first and second terms indicate the Zeeman interaction and a fine interaction, respectively. It can be estimated from the angular dependence that g-values are ≈2.003 for the T6 signal and ≈2.01 for the T7 signal, whereas accurate components of g-tensor for both the signals could not be determined because of a superposition of the T1, T5, and other unknown ESR lines on the T6 and T7 signals. Anisotropies of ESR lines for the T6 and T7 signals are described by axially symmetric D tensors along the ⟨111⟩ axis: The absolute values of D are derived to be 1.2×10^{-2} and $5.2 \times 10^{-2}\,\mathrm{cm}^{-1}$ for the T6 and T7 signals, respectively, which are denoted in Table 1. Using these g and D values, the angular dependences obtained for the T6 and T7 signals are well described by the calculated curves, as shown in Fig. 8, where the rotation axis was misaligned at 3.5°. The axially symmetric D tensors suggest that two electron spins, which interact with each other, are aligned along ⟨111⟩ directions. When we assume that the fine structures are mainly due to the magnetic dipole–dipole interaction, the value of D is represented as

$$D = -\frac{3}{2}\left[\frac{\mu_0(g\beta)^2}{4\pi r^3}\right], \tag{6}$$

where r is the average distance of two electron spins. From the obtained absolute values of D, the average spin–spin distances are estimated to be 6.1 and 3.8 Å for the T6 and T7 centers, respectively. Taking account of the bond length of Si–C (1.89 Å) in 3C-SiC, the average distances of electron spins in the T6 and T7 centers are approximately 3.2 and 2 times as long as the Si–C bond length.

Now we consider the structures for the T6 and T7 centers. The introduction rates of the T6 and T7 centers were obtained to be 3.4×10^{-1} and $1.9 \times 10^{-2}\,\mathrm{cm}^{-1}$, respectively, for 1 MeV electron irradiation. These values are not smaller than the introduction rate of the T1 center ($1.7 \times 10^{-2}\,\mathrm{cm}^{-1}$) and much larger than that for divacancies in Si ($\approx 4 \times 10^{-3}\,\mathrm{cm}^{-1}$) [39]. This fact indicates that the T6 and T7 centers are simple point defects produced primarily by electron irradiation like V_{Si}, V_C, and Frenkel pairs (vacancy–interstitial pairs: V_{Si}–I_{Si} and V_C–I_C). Since no hfs caused by ^{27}Al, ^{14}N, and ^{1}H was observed, the possibility that impurities are incorporated in the T6 and T7 structures is very low, suggesting that these centers are intrinsic defects. The T6 and T7 signals were not observed clearly in p-type samples irradiated with 2 MeV protons unlike the case of 1 MeV electron irradiation. This result indicates the preferential formation of these defects by electron irradiation. In 1 MeV electron irradiation, the average energy of primary knock-on atoms (PKAs) is estimated to be ≈50 eV, which is of the same order as the displacement energy $E_d = 27$ eV [40]. On the other hand, the average PKA energy transferred from 2 MeV protons is ≈300 eV, which is much higher than E_d. Thus, in the electron irradiation, PKAs can be located near the vacancy sites from where they were displaced, and much more Frenkel pairs are created compared with 2 MeV proton irradiation. Taking all the results into account, Frenkel pairs are most plausible for the T6 and T7 structures. On the basis of the axially symmetric D tensor obtained, an interstitial atom is deduced to be located in the ⟨111⟩ direction from a vacancy. In addition, it is derived from the average spin–spin distance obtained for each center that an interstitial atom is located at the nearest-neighbor tetrahedral interstitial site around a vacancy for the T7 center, and at the second-nearest tetrahedral interstitial site for the T6 center. As for interstitials in 3C-SiC, Nashiyama et al. [23] showed

the location of displaced C atoms at tetrahedral interstitial sites from deuteron channeling experiments. This result supports our model. However, we could not specify the correspondence of V_{Si}–I_{Si} and V_C–I_C pairs to the T6 and T7 centers owing to lack of information on ^{29}Si and ^{13}C hf structures. Then, the T6 and T7 signals were not observed in n-type samples. This result can be explained by the assertion that these defects are not paramagnetic in n-type samples due to the change in their charge state. Gap states of such vacancy–interstitial pairs were also predicted theoretically [4].

3.2 Vacancy-type defects: positron traps

3.2.1 Defects detected by Doppler broadening spectroscopy

Fig. 9 shows the measured values of the S parameter as a function of incident positron energy for n-type 3C-SiC samples irradiated with 1 MeV electrons. The data for the unimplanted sample is also shown. The mean implantation depth Z (in nm) of positrons with an acceleration energy E (in keV) is given by $Z = (33.2/\varrho)\, E^{1.6}$, where ϱ is the mass density of 3C-SiC (in g/cm^3) ($\varrho = 3.21$ g/cm^3). The mean implantation depth of positrons is also indicated in the upper abscissa in Fig. 9. Then, the dependence of the S parameter on positron energy $S(E)$ is represented by a superposition of the characteristic S parameters for positron annihilations at the surface (S_s) and those in the sample interior (S_{int}),

$$S(E) = F_s(E)\, S_s + [1 - F_s(E)]\, S_{int}\,, \tag{7}$$

where $F_s(E)$ is the fraction of positrons diffusing back to the surface.

In the positron energy range below ≈5 keV, the measured S value increased with decreasing positron energy, which is caused by outdiffusion of positrons and their annihilation at the surface. Above ≈10 keV, the S values was independent of incident positron energy. This represents that almost all positrons annihilate in the bulk without their diffusion back to the surface. In this case, the surface contribution is negligible and the measured S values correspond to S_{int}. For as-grown 3C-SiC epilayers, the positron diffu-

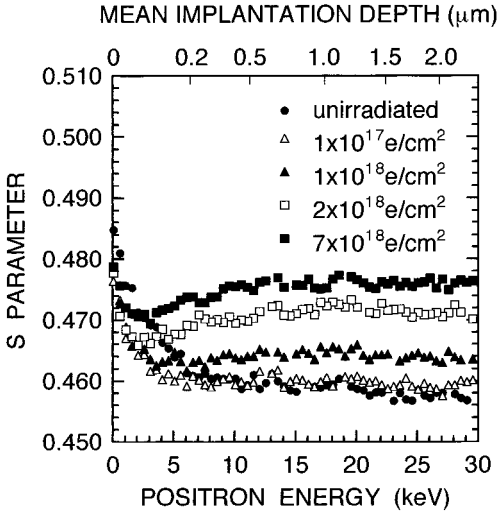

Fig. 9. S parameter as a function of incident positron energy for unirradiated and electron irradiated 3C-SiC samples. The mean implantation depth of positrons is also shown in the upper abscissa

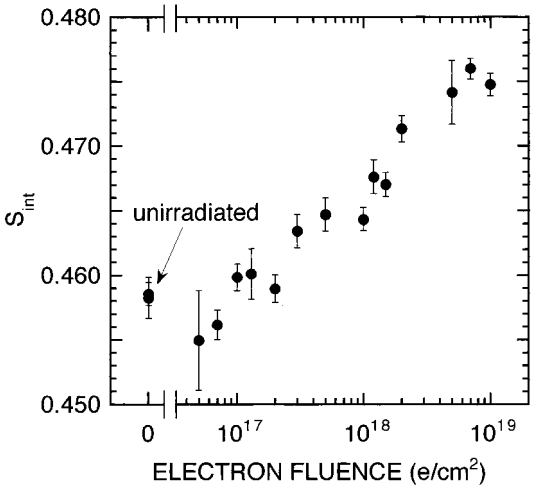

Fig. 10. Electron fluence dependence of the characteristic S parameter (S_{int}) in the interior region of 3C-SiC

sion length was obtained to be 184 nm from recent $S(E)$ data [41]. This value agrees well with that reported for defect-free Si [42], indicating that almost all positrons annihilate from the free state in unirradiated 3C-SiC. In the electron irradiated samples, the defects produced are distributed homogeneously and thus the S_{int} values are constant in the bulk region.

Fig. 10 shows the dependence of S_{int} on electron fluence. The value of S_{int} increased with electron fluence, showing that vacancy-type defects which trap positrons are introduced in 3C-SiC by electron irradiation. It was found that V_{Si}^{-} is created in 3C-SiC by such particle irradiation, as described in Section 3.1.1. Similarly, V_C and interstitials are presumably produced by electron irradiation. Positrons are known to be hardly trapped by interstitial-type defects. It was reported from PAS measurements of GaAs that positrons were not captured effectively by vacancies at arsenic sites and by antisite defects [43, 44]. In analogy to this result, V_C as well as antisite defects in 3C-SiC can be regarded as ineffective positron traps. Recent PAS studies of electron irradiated 6H-SiC also indicated that V_C is essentially invisible in Doppler broadening experiments [45]. Therefore, the increase in S_{int} observed by electron irradiation is attributed to the formation of V_{Si}^{-}, which forms an attractive potential for positrons due to its negative charge state.

When defects trapping positrons are introduced in a material, S_{int} is expressed by a competition between annihilations in the bulk (S_{b}) and in the defects (S_{d}),

$$S_{\mathrm{int}} = \frac{\lambda S_{\mathrm{b}} + \varkappa S_{\mathrm{d}}}{\lambda + \varkappa} \,, \tag{8}$$

where λ is the free positron annihilation rate and $\varkappa$ the net trapping rate of positrons into the defects. The latter is proportional to the concentration of defects C_{d}: $\varkappa = \mu C_{\mathrm{d}}$, where μ is the specific trapping rate. Since S_{d} is larger than S_{b}, the introduction of positron traps like vacancy-type defects raises the value of S_{int}, and finally S_{int} approaches S_{d}. Here, the ratio of S_{d} to S_{b} gives information about the size of vacancy-type defects. The relation between the ratio $S_{\mathrm{d}}/S_{\mathrm{b}}$ and the defect species has been established for Si, e.g., $S_{\mathrm{d}}/S_{\mathrm{b}} = 1.03$ for monovacancies and $S_{\mathrm{d}}/S_{\mathrm{b}} = 1.04$ to 1.06 for divacancies V_2

in Si [42, 46 to 48]. From the fluence dependence of S_{int}, the ratios of the S_{int} values for the samples irradiated at fluences above $\approx 5 \times 10^{18}\,\mathrm{e/cm^2}$ to that for the unirradiated one are estimated to be ≈1.04, which is close to the value reported for V_2 for Si. This implies that V_2 as well as V_{Si} are produced in 3C-SiC by 1 MeV electron irradiation at such high fluences. A fitting result obtained by assuming the production of both V_{Si} and V_2, was reported in a previous paper [30]. However, the relation between the ratio $S_{\mathrm{d}}/S_{\mathrm{b}}$ and the defect species has not yet been made clear for SiC and information on the defect species obtained from Doppler broadening spectra is rather limited. In order to confirm the formation of V_2, further investigations using positron lifetime measurements are necessary. In the next section, the positron lifetime results newly obtained for electron irradiated 3C-SiC will be shown. From the Doppler broadening measurements of electron irradiated 3C-SiC, it can be concluded the V_{Si}^{-} is produced by electron irradiation and that it is responsible for the increase in the S parameter.

3.2.2 Defects detected by positron lifetime spectroscopy

Fig. 11 shows typical lifetime spectra of positrons annihilated in unirradiated and electron irradiated 3C-SiC samples (unintentionally doped, n-type). The lifetime spectrum $L(t)$ was decomposed into two lifetime components as follows:

$$L(t) = \frac{I_1}{\tau_1} \exp\left(-\frac{t}{\tau_1}\right) + \frac{I_2}{\tau_2} \exp\left(-\frac{t}{\tau_2}\right), \tag{9}$$

where τ_i and I_i are the lifetime and the intensity of the i-th component, respectively, where $I_1 + I_2 = 1$. Assuming that positrons annihilate through the free state in the bulk and the trapped state at vacancy-type defects, which is called the two-state trapping model, the lifetimes τ_1 and τ_2 are described as

$$\begin{aligned} \tau_1 &= \frac{1}{\tau_{\mathrm{b}}^{-1} + \varkappa}\,, \\ \tau_2 &= \tau_{\mathrm{v}}\,. \end{aligned} \tag{10}$$

Here, τ_{b} and τ_{v} represent the positron lifetimes in the bulk and at vacancy-type defects, respectively. $\varkappa$ is the net positron trapping rate at the defects and denoted as $\varkappa = (I_2/I_1)\,(\tau_{\mathrm{b}}^{-1} - \tau_2^{-1})$. The validity of the analysis based on the two-state trap-

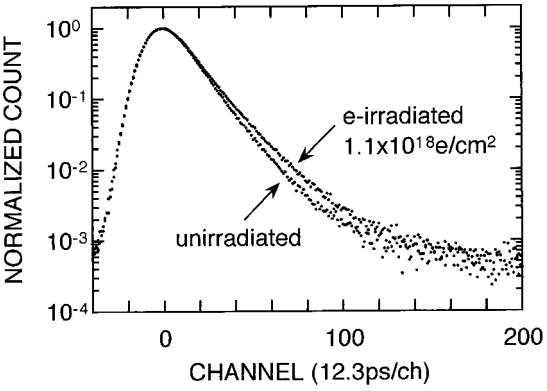

Fig. 11. Positron lifetime spectra for n-type 3C-SiC samples before and after 1 MeV electron irradiation. The electron fluence in the irradiated sample was $1.1 \times 10^{18}\,\mathrm{e/cm^2}$

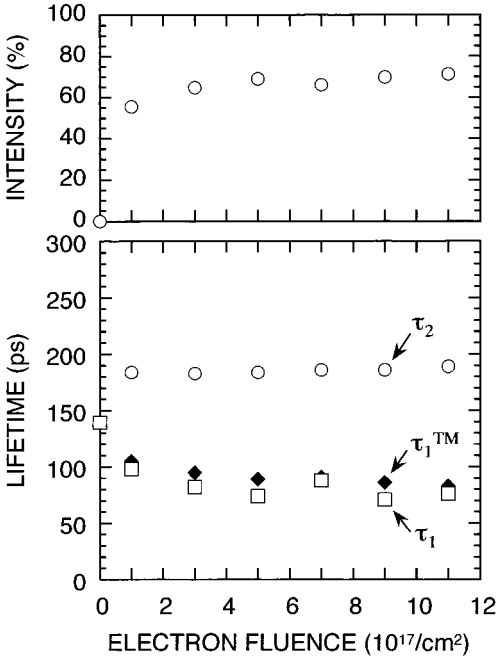

Fig. 12. Positron lifetimes τ_1 and τ_2, and intensity I_2 as functions of electron fluence for 3C-SiC irradiated with 1 MeV electrons. The calculated lifetime τ_1^{TM} is also shown

ping model can be examined by the difference between τ_1 determined by eq. (9) and that calculated using eq. (10). For the unirradiated sample, only one lifetime component of 139ps was obtained. Similar values were reported for high quality 6H-SiC [45, 49] and also derived theoretically for 3C and 6H-SiC [50]. Therefore, this value can be regarded as τ_{b} for 3C-SiC. It is shown from Fig. 11 that the positron lifetime increases by electron irradiation, giving an evidence for the introduction of vacancy-type defects in 3C-SiC by irradiation.

Two lifetime components τ_1 and τ_2 and the intensity I_2 derived by decomposition of the lifetime spectra using eq. (9) are shown in Fig. 12 as a function of electron fluence. The lifetime τ_1^{TM} calculated by eq. (10) is also represented in this figure. The fact that the τ_1 value agrees well with the τ_1^{TM} value at every fluence assures the validity of the analysis based on the two-state trapping model. Thus, the lifetimes τ_1 and τ_2 correspond to those for positron annihilation in the bulk and at vacancy-type defects, respectively. The lifetime τ_2 is found to exhibit an almost constant value (186 ± 4) ps in the fluence range up to 1.1×10^{18} e/cm^2. This value is in good agreement with the positron lifetimes at V_{Si} calculated recently for 3C-SiC: $\tau_{\mathrm{v}} = 191$ and 185ps were calculated using the tight-binding linear muffin-tin orbital method and the atomic superposition method, respectively [50, 51]. Consequently, V_{Si} is confirmed to be generated in 3C-SiC by electron irradiation and act as a main positron trap. This conclusion agrees to that derived from the Doppler broadening and ESR results. Taking account of a negative charge state of V_{Si} in n-type 3C-SiC, it is found experimentally that the lifetime is (186 ± 4) ps for positron annihilation at V_{Si}^{-} in 3C-SiC.

Similarly to the result that V_C was invisible in the Doppler broadening measurements, the lifetime component corresponding to positron annihilations at V_C was not observed apparently. As for the reason why it was not detected, two possibilities can be considered: The first is that almost all V_C is annealed out during irradiation. On the basis of the fact that V_C^{+} was annealed out at $\approx 400\,^{\circ}$C (see Section 3.3), this possibility is believed to be low. The second is that the trapping rate of positrons at V_C is low and insufficient to be detected by positron lifetime measurements. The net positron trapping rate at defects depends not only on the defect concentration but also on the charge state and the mean volume of the defects [34]. In contrast to a negative charge state of V_{Si},

the charge state of V_C was deduced from the ESR results to be neutral in n-type 3C-SiC. In addition, the mean volume of V_C is considered small compared with V_{Si}. These facts probably make V_C^0 undetected. Theoretical calculation indicated that the lifetime at V_C in 3C-SiC was 150 ps [50, 51], which is similar to the bulk lifetime ($\tau_b = 139$ ps). This may lead to an additional problem in the discrimination of the V_C component from the bulk one. It was suggested from the Doppler broadening results that V_2 was formed in 3C-SiC by 1 MeV electron irradiation at high fluences like 1×10^{19} e/cm^2. Since the positron lifetime at V_2 is longer than that at V_{Si}, the formation of V_2 should be detected by lifetime measurements. In fact, by using positron lifetime technique, the introduction of V_2-type defects was reported for n-type 6H-SiC irradiated with 3 MeV electrons [49] or 200 keV Ge ions [51]. However, this problem could not be solved by the present lifetime measurements up to a fluence of 1.1×10^{18} e/cm^2. To examine the formation of V_C and V_2, successive studies are now in progress. It can be concluded from the lifetime results that V_{Si}^- is the main positron trap exhibiting the characteristic positron lifetime 186 ps.

3.3 Annealing behavior of point defects: defect interaction

Fig. 13a shows isochronal annealing of the T1 center, i.e., V_{Si}^- in n-type 3C-SiC samples irradiated with 1 MeV electrons. The T1 center was found to be annealed at three stages, 150, 350, and 750 °C [24], which are indicated by arrows in Fig. 13a. A similar annealing result was obtained for the T1 center in n-type samples irradiated with 2 MeV protons, which is shown in Fig. 13b. At the highest stage, annealing of the T1 center was represented by a first-order reaction with an activation energy 2.2 eV [24]. From

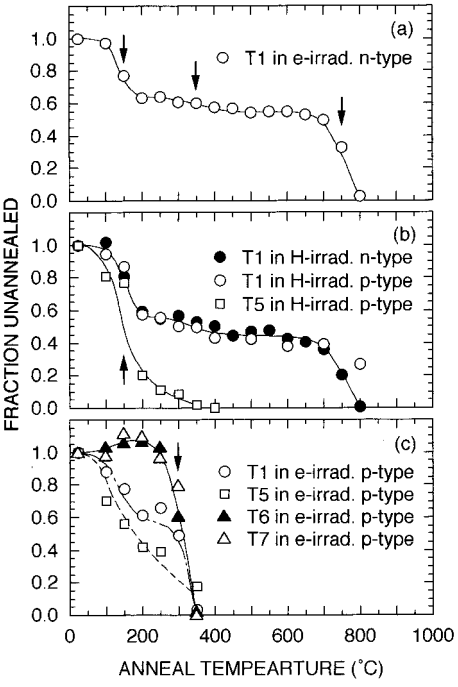

Fig. 13. Isochronal annealing of ESR centers in a) n-type 3C-SiC irradiated with 1 MeV electrons, b) n- and p-type 3C-SiC irradiated with 2 MeV protons, and c) p-type 3C-SiC irradiated with 1 MeV electrons. Annealing stages of the T1, T5, and the other centers (T6 and T7) are represented by arrows in a), b), and c), respectively. Fluences were 3×10^{18} and 5×10^{17} e/cm^2 in the electron irradiated n-type and p-type samples, respectively, and 1×10^{16} and 1×10^{15} H$^+$/cm^2 in the proton irradiated n-type and p-type samples, respectively

this result, it was deduced that at this stage V_{Si}^{-} walks randomly and disappears at a sink, which might be related to extended defects like dislocations. Almost the same annealing stage was reported for the F center [14], which was found to be identical with the T1 center [25], in bulk 3C-SiC and 6H-SiC irradiated with electrons and neutrons. At the lower stages, it is likely that this defect disappears through the combination with other radiation induced defects such as interstitials. Similar stages of 150 and 300 °C were also found from a change in resistivity due to annealing for neutron irradiated 3C-SiC epilayers [20, 21] and bulk SiC [52]. As for the combination of vacancies and interstitials, Kawasuso et al. [49] reported recently that radiation induced vacancy-type defects were combined with interstitials in 6H-SiC by annealing up to 500 °C. Theoretical studies also indicated the annihilation of V_{Si} via the combination with interstitials [6]. Thus, it is likely that interstitials play an important role in annealing of V_{Si} at low temperatures.

The result of isochronal annealing of the T5 center [27] as well as the T1 center in p-type 3C-SiC samples irradiated with 2 MeV protons is shown in Fig. 13b. Disappearance of the T5 center, i.e. V_C^{+}, started at 100 °C and about 80% of the initial amount was lost after 200 °C annealing. An annealing stage for the T5 center is represented by the arrow in the figure. Additional ESR signals were not produced by thermal annealing at temperatures around 150 °C. These results indicate the possibility that V_C^{+} moves to combine with other defects, which are considered a sink, and forms non-paramagnetic complexes or that it disappears through the combination with interstitials mobile at this stage. The T1 center in these samples exhibits similar annealing behavior as in n-type samples. One can image that V_C combines with V_{Si} around 150 °C from the fact that both the T5 and T1 centers disappear at this temperature. However, recent PAS measurements of 6H and 3C-SiC isochronally annealed after electron irradiation showed no apparent increase in the positron lifetime up to 1500 °C [49, 53]. Thus, the possibility of the combination between V_C and V_{Si}, which leads to the formation of V_2, is thought to be quite low. This supports our speculation that V_C disappears via the capture by a sink or the combination with interstitials.

Annealing of the T6 and T7 centers in p-type 3C-SiC samples irradiated with 1 MeV electrons is shown in Fig. 13c. In this figure, the results for the T1 and T5 centers in the same sample are also shown. As a result, the T6 and T7 centers are found to be annealed at temperatures around 300 °C. When we regard them as Frenkel pairs, annealing of these defects is probably ascribed to the recombination or the dissociation of vacancy–interstitial pairs. The dissociation of vacancy–interstitial pairs should be associated with the formation of isolated vacancies. However, no significant increase in the T1 and T5 centers was observed around 300 °C. Thus, the recombination of vacancy–interstitial pairs is preferable as the annealing mechanism of the T6 and T7 centers. At temperatures below ≈200 °C, slight increases in the T6 and T7 centers due to annealing are seen. This might be related to additional coupling of mobile interstitials with vacancies, which is consistent with the explanation for the annealing of the T1 and T5 centers. In contrast to the annealing results in the other samples, the T1 center is found to disappear after 350 °C annealing. This result can be explained in terms of a change in the charge state of $V_{Si} : V_{Si}^{-}$ is altered to non-paramagnetic V_{Si}^{0} due to lowering of the Fermi level in p-type 3C-SiC, because most of defects, which involve the T6 and T7 centers, are annealed out around 300 °C. The position of a V_{Si} level in the 3C-SiC band gap is discussed in Section 4.3. On the other hand, this anomalous disappearance of the

T1 center was not observed in p-type samples irradiated with 2 MeV protons. In the case of the proton irradiation, a number of defects are created and these defects retard the shift of the Fermi level.

4. Effects of Defects on Electrical and Optical Properties

4.1 Electrical properties

In order to examine the effects of intrinsic point defects on the electrical properties of 3C-SiC, Hall measurements were performed for n-type 3C-SiC irradiated with 1 MeV electrons [36]. The carrier (electron) concentration and the Hall mobility at RT as a function of electron fluence are shown in Fig. 14. Both the carrier concentration and mobility decreased with increasing electron fluence. The removal rate of carriers is estimated from this result to be $1.4 \times 10^{-2}\,\mathrm{cm}^{-1}$. This value agrees well to the introduction rate of the T1 center ($1.7 \times 10^{-2}\,\mathrm{cm}^{-1}$). Moreover, it was found from isochronal annealing that the recovery stages of the carrier concentration were in good agreement with those for the T1 center [36]. These results show that V_{Si} acts as a predominant electron trap in n-type 3C-SiC. The behavior of V_{Si} as an acceptor was also predicted theoretically [6 to 8]. The temperature dependence of the Hall mobility indicated that some electron scattering centers performing like ionized impurities were introduced in 3C-SiC by electron irradiation [37]. This result can be interpreted by the assertion that the T1 center, i.e. V_{Si}^{-}, scatters electrons effectively at low temperatures.

It was reported that the resistivity of n-type 3C-SiC epilayers increased by fast neutron irradiation, which was mainly due to the introduction of deep-level defects [20, 21]. The carrier removal rate was estimated from the change in the resistivity to be $7.2\,\mathrm{cm}^{-1}$ (for 1 MeV equivalent neutron). Heavier particles or higher-energy particles produce higher concentrations of defects. In fact, the value of $2.7 \times 10^{2}\,\mathrm{cm}^{-1}$ was obtained for the introduction rate of the T1 center in 2 MeV proton irradiation [25]. In addition, most of deep-level defects produced by neutron irradiation were reported to be annealed at temperatures up to 350 °C [20, 21]. Annealing at such low temperatures was also observed for the ESR centers arising from intrinsic defects, as represented in the former section. Thus, it is most probable that intrinsic point defects like V_{Si} act as effective electron traps in neutron and proton irradiated epilayers as in the case of electron irradiation. On the other hand, to our knowledge, no data has been reported on the influ-

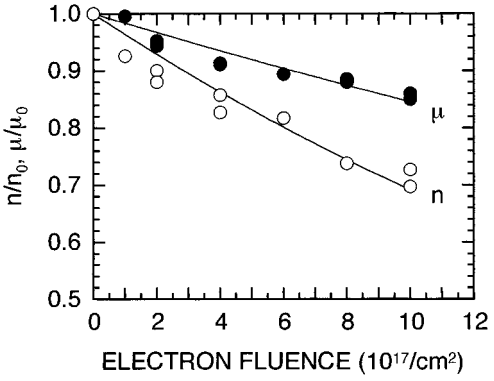

Fig. 14. Carrier density n and Hall mobility μ at room temperature in electron irradiated n-type 3C-SiC. n_0 and μ_0 indicate the carrier density and the Hall mobility before irradiation

ence of the defect introduction on the hole concentration and its mobility in p-type 3C-SiC. Such information in p-type 3C-SiC is indispensable for a comprehension of the effects of intrinsic point defects on the electrical properties of SiC bipolar devices.

4.2 Optical properties

Fig. 15 shows a typical PL spectrum at 4 K for n-type 3C-SiC irradiated with electrons. PL lines induced by irradiation were observed mainly in the photon energy range below 2.0 eV. A dominant PL line labeled E appeared at 1.913 eV [31] with a full width at half maximum of ≈2.5 meV at 4 K. In addition, radiation induced PL lines D_1 (1.973 eV), α_1 (1.964 eV), α_2 (1.959 eV), β_1 (1.955 eV), β_2 (1.954 eV), and γ (1.893 eV) were found at 4 K, as indicated in Fig. 15. At temperatures around 50 K, another PL line δ at 1.922 eV which was induced by irradiation was also observed. In the energy range between 2.1 and 2.4 eV, sharp PL lines attributed to phonon replicas of impurity bound excitons (BEs) [54, 55] were observed, and their intensity was weakened by electron irradiation. Geiczy et al. [15, 16] performed CL measurements at 100 K for bulk 3C-SiC irradiated with 3.5 MeV electrons. They reported defect related zero phonon lines (ZPLs) A_0 (1.970 eV), B_0 (1.953 eV), C_0 (1.911 eV), and D_0 (1.889 eV). The D_1, α_1 (and/or α_2), E, and γ PL lines observed in this experiment correspond to the A_0, B_0, C_0, and D_0 CL lines, respectively, where the D_1 line was already reported to arise from the same defect as the A_0 CL line [17 to 19, 54]. Since almost the same annealing behavior was observed between α_1 and α_2 lines and also between β_1 and β_2 lines, each PL line pair is attributable to the same defect species. The PL lines observed here are presumably caused by simple point defects introduced primarily by electron irradiation because large aggregates of defects are less likely to exhibit such sharp PL lines.

Fig. 16 shows the change in the intensity of these PL lines due to isochronal annealing. The annealing result of the BE–TO(X) phonon replica (2.282 eV) is also shown in Fig. 16c. It was found that the intensity of the E ZPL decreased apparently by 200 and 700 °C annealing. After 800 °C annealing, this line completely disappeared. In contrast to the annealing of this line, the other PL lines induced by electron irradiation as well as the BE related lines were not changed significantly up to ≈800 °C. This result indicates

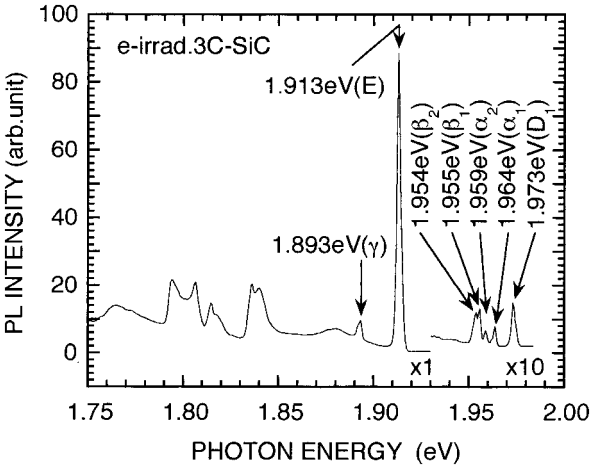

Fig. 15. PL spectrum at 4 K for 3C-SiC irradiated with 1 MeV electrons at 2×10^{17} e/cm^2. PL lines induced by irradiation are presented by arrows with the photon energies

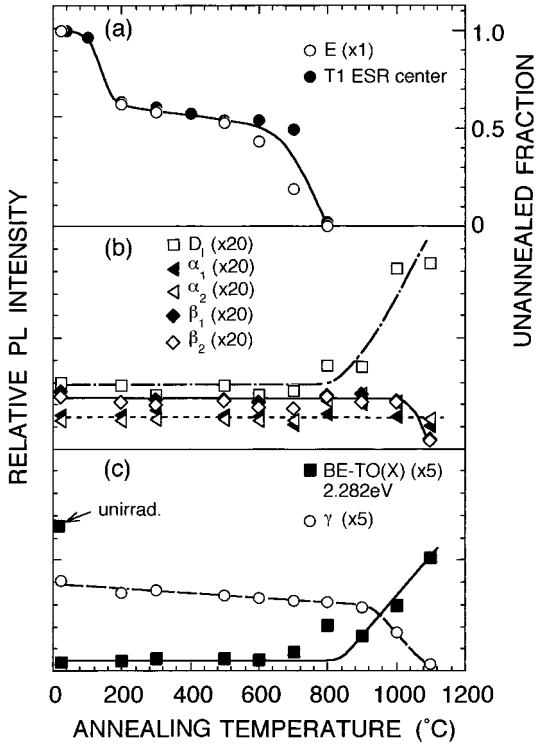

Fig. 16. Isochronal annealing effects on the intensity of PL lines a) E (1.913 eV), b) D_1 (1.973 eV), α_1 (1.964 eV), α_2 (1.959 eV), β_1 (1.955 eV), β_2 (1.954 eV), and c) γ (1.893 eV) in electron irradiated 3C-SiC. Annealing of the T1 center is also shown in a). Recovery of the BE–TO(X) line is indicated in c)

that the observed decrease in the E ZPL is caused by the elimination of a defect exhibiting the E ZPL but not by the generation of other recombination channels. The result of annealing for the T1 center is also shown in Fig. 16a for comparison. The annealing behavior of the E PL center agrees well with that for the T1 center arising from V_{Si}^-: The annealing stages and the fraction annealed at each stage for the E PL center correspond well to those for the T1 center. In addition, the activation energy 2.2 eV for annealing of the T1 center around 750 °C is almost the same as the value obtained for the C_0 CL center [15] which is identical with the E PL center. Consequently, the E PL line is concluded to arise from V_{Si}. As for the other PL lines, they were still observed after annealing at 1000 °C: The β and γ PL lines disappeared around 1000 °C. No significant change was observed in the intensity of the α PL lines. The intensity of the D_1 line increased at temperatures above ≈800 °C. Considering these results in conjunction with the annealing results of ESR centers, it is expected that these PL centers correspond to neither V_C nor Frenkel defects. Some of them might be related to impurities.

Regarding recent luminescence studies, Son et al. [32] performed PL and ODMR measurements of electron irradiated 3C-SiC epilayers, and found an ODMR signal labeled L2 having an isotropic g-value 2.0061 ± 0.0002 with $S = 1/2$. This defect was reported to act as a carrier recombination center which accompanies a PL band at 1.121 eV. From the fact that this defect started to migrate at 750 °C and disappeared completely at 900 °C, the L2 center was concluded to be related to V_{Si}. At annealing temperatures above ≈800 °C, the D_1 and D_2 PL lines [17 to 19] became dominant. The intensity of these PL lines was shown by Freitas et al. [22] to increase up to 1600 °C. It was also reported that above 1600 °C the D_2 line intensity dropped rapidly while the D_1 line intensity was not changed up to 1760 °C. Whereas the origins of the D_1 and D_2 PL lines were supposed by Choyke et al. [17 to 19] to be divacancies and carbon di-interstitials, respectively, they have not yet been clarified up to now. In contrast to the proposed model of the D_1 center, Vainer and Ilin [56] suggested that this PL line was attributed

to V_{Si}–N complexes. Recent PAS studies by Kawasuso et al. [49] showed that the D_1 PL line was independent of vacancies. Further investigations are required to identify the structure of such PL centers.

4.3 Electronic levels

Assuming that the E ZPL is caused by radiative recombination of exited carriers between a defect state of V_{Si} and the band edge of 3C-SiC, we can estimate an electronic level of V_{Si} in 3C-SiC. It was clarified from ESR that V_{Si} has a negative charge in n-type and p-type 3C-SiC samples irradiated with electrons or protons. This shows that a V_{Si} level is located in the lower half of the 3C-SiC band gap. Taking account of the band gap (2.417 eV) [57], the photon emission of 1.913 eV is attributable to the radiative transition between the bottom of the conduction band and an electronic level of V_{Si}. Therefore, a defect level of V_{Si} is considered to be located at 0.50 eV above the top of the valence band ($E_v + 0.50$ eV). The electronic level of V_{Si} is schematically shown in Fig. 17a. On the other hand, from the fact that V_C^+ was observed in p-type samples but not in n-type samples, its level can be estimated to exist in a position above the V_{Si} level whereas its exact location cannot be determined (Fig. 17a). These estimated positions agree with the theoretical prediction by Talwar and Feng [8] and Wang et al. [6], which is stated below.

Some calculated defect levels are also shown in Fig. 17b. It was shown theoretically that V_{Si}, V_C, V_2 (V_{Si}–V_C) have gap states in 3C-SiC. As a result of calculations based on the tight-binding formalism using a Green's function theory, Talwar and Feng [8] showed that V_{Si} with a level $E_v + 0.54$ eV and V_C with $E_v + 1.66$ eV act as acceptors and donors, respectively. This result is in agreement with the results derived by Wang et al. [6] using a pseudopotential method. Our estimated level of V_{Si} is almost the same as that derived theoretically. Concerning V_2, two levels at $E_v + 0.48$ eV and $E_v + 1.62$ eV were derived by Talwar and Feng [8]. Similar values of $E_v + 0.38$ eV and $E_v + 1.62$ eV were obtained by Li and Lin-Chung [5]. In addition, it was shown that

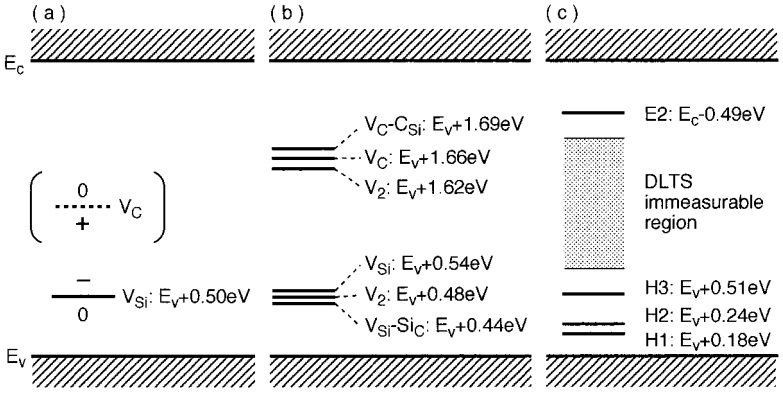

Fig. 17. Schematic representation of the electronic levels of point defects in 3C-SiC. a) An electronic level of V_{Si} and a possible position of a V_C level estimated from our PL data, b) theoretically predicted levels of V_{Si}, V_C, V_2, and vacancy–antisite pairs (from [8]), and c) several levels obtained by DLTS for neutron irradiated 3C-SiC (from [21]). In Fig. 17a, the signs + and – represent the charge states of V_{Si} and V_C

neither antisite Si_C nor C_{Si} has an electrically active level in the band gap of 3C-SiC [4 to 8]. Experimentally, Nagesh et al. [20, 21] reported several DLTS peaks in neutron irradiated 3C-SiC epilayers. The positions of E2, H1, H2, and H3 levels, which were caused by point defects induced by irradiation, are represented schematically in Fig. 17c. The E2 center was shown to grow in magnitude with increasing temperature up to 350 °C, whereas the total defect concentration decreased. From this result and the fact that such increase was not observed in any ESR centers, the E2 center can be ascribed to some defect complexes different from the T1, T5, T6, and T7 centers. On the other hand, the H1, H2, and H3 centers were annealed up to ≈350 °C [21]. Most ESR centers were also annealed partly or completely in such a temperature range. Thus, some of these electronic levels may be attributed to the intrinsic point defects found by ESR. Actually, our estimated V_{Si} level is close to the DLTS level H3. Nevertheless, since experimental data available at the present stage is insufficient to assign electronic levels to the defect structures, further experimental studies are needed to clarify the electronic levels of intrinsic defects.

5. Summary

For a microscopic understanding of intrinsic point defects, ESR and PAS have been performed for single crystalline 3C-SiC, which was epitaxially grown on Si by CVD, irradiated with fast particles such as 1 MeV electrons and 2 MeV protons. Several ESR signals resulting from point defects were found in n-type and p-type samples irradiated. As a consequence of the analysis of ESR data using a spin Hamiltonian, two fundamental intrinsic defects V_{Si}^- and V_C^+ have been identified: V_{Si}^- has T_d symmetry with an effective spin $S = 3/2$, and V_C^+ has D_2 symmetry with $S = 1/2$. A series of ESR studies also indicated the presence of two kinds of Frenkel defects, i.e., vacancy–interstitial pairs with $S = 1$, in which an interstitial atom is located at a tetrahedral interstitial site in the $\langle 111 \rangle$ direction from a vacancy. Increases in the S parameter and the positron lifetime by electron irradiation, which have been found by using Doppler broadening and positron lifetime spectroscopy, give the evidences for the formation of V_{Si}^-. The positron lifetime at V_{Si}^- has been shown experimentally to be 186 ps. Annealing of V_{Si}^- was found to take place at three stages 150, 350, and 750 °C. At the highest stage, V_{Si}^- is considered to be mobile and trapped by a sink. It was also shown that V_C^+ disappears at temperatures around 150 °C, and that two vacancy–interstitial pairs are annealed at 300 °C.

The effects of intrinsic point defects on the electrical and optical properties of 3C-SiC have been investigated using Hall and PL measurements. It was found that in n-type 3C-SiC, V_{Si} behaves as a predominant electron trap and an effective carrier scattering center at low temperatures. In addition, it was shown from the analysis of the PL results in connection with the ESR results that V_{Si} acts as a radiative recombination center associated with an emission of photons with an energy 1.913 eV. An electronic level of V_{Si} was estimated to be $E_v + 0.50$ eV. Besides this 1.913 eV photon emission, several PL lines arising from point defects have been found in irradiated 3C-SiC. These PL lines were suggested to have no correlation with the ESR centers shown above.

Though fast particle irradiation primarily introduces interstitials as well as vacancies, no direct evidence has been given for the presence of isolated interstitials. Similarly, experimental data proving the formation of antisite defects Si_C and C_{Si} has not yet been obtained whereas they are expected to be produced in 3C-SiC by irradiation and/or

subsequent annealing. Recent studies using PL, DLTS, and ODMR and theoretical investigations of defects in 3C-SiC have given much information about the nature of defects. However, in order to clarify the structure, electronic levels, and annealing kinetics of intrinsic defects like interstitials, antisites, and divacancies, further investigations are required. Knowledge of intrinsic defects in SiC makes a contribution to not only improving SiC crystal quality but also designing fabrication processes of SiC devices.

References

[1] See, for example, papers dealing with SiC devices in section E of this special issue.
[2] P. Das and D. K. Ferry, Solid State Electronics **19**, 851 (1976).
[3] W. E. Nelson, F. A. Halden, and A. Rosengreen, J. Appl. Phys. **37**, 333 (1966).
[4] P. J. Lin-Chung and Y. Li, Mater. Sci. Forum **10/12**, 1247 (1986).
[5] Y. Li and P. J. Lin-Chung, Phys. Rev. B **36**, 1130 (1987).
[6] C. Wang, J. Bernholc, and R. F. Davis, Phys. Rev. B **38**, 12752 (1988).
[7] J. Bernholc, S. A. Kajihara, C. Wang, and A. Antonelli, Mater. Sci. Engng. B **11**, 265 (1992).
[8] D. N. Talwar and Z. C. Feng, Phys. Rev. B **44**, 3191 (1991).
[9] S. Nishino, J. W. Powell, and H. A. Hill, Appl. Phys. Lett. **42**, 460 (1983).
[10] S. Yoshida, K. Endo, E. Sakuma, S. Misawa, H. Okumura, H. Daimon, E. Muneyama, and M. Yamanaka, Mater. Res. Soc. Symp. Proc. **97**, 259 (1987).
[11] P. Liaw and R. F. Davis, J. Electrochem. Soc. **132**, 642 (1985).
[12] S. Nishino, H. Suhara, H. Ono, and H. Matsunami, J. Appl. Phys. **61**, 4889 (1987).
[13] J. Schneider and K. Maier, Physica B **185**, 199 (1993) (and references therein).
[14] L. A. de S. Balona and J. H. N. Loubser, J. Phys. C **3**, 2344 (1970).
[15] I. I. Geiczy, A. A. Nesterov, and L. S. Smirnov, in: Radiation Effects in Semiconductors, Ed. J. W. Corbett and G. D. Watkins, Gordon & Breach, London 1971 (p. 327).
[16] I. I. Geiczy, A. A. Nesterov, and L. S. Smirnov, Soviet Phys. – Semicond. **4**, 744 (1970).
[17] W. J. Choyke and L. Patrick, Phys. Rev. B **4**, 1843 (1971).
[18] L. Patrick and W. J. Choyke, J. Phys. Chem. Solids **34**, 565 (1973).
[19] W. J. Choyke, Inst. Phys. Conf. Ser. No. 31, 58 (1977).
[20] V. Nagesh, J. W. Farmer, R. F. Davis, and H. S. Kong, Appl. Phys. Lett. **50**, 1138 (1987).
[21] V. Nagesh, J. W. Farmer, R. F. Davis, and H. S. Kong, Radiat. Effects and Defects in Solids **112**, 77 (1990).
[22] J. A. Freitas, Jr., S. G. Bishop, J. A. Edmond, J. Ryu, and R. F. Davis, J. Appl. Phys. **61**, 2011 (1987).
[23] I. Nashiyama, T. Nishijima, E. Sakuma, and S. Yoshida, Nuclear Instrum. and Methods B **33**, 599 (1988).
[24] H. Itoh, N. Hayakawa, I. Nashiyama, and E. Sakuma, J. Appl. Phys. **66**, 4529 (1989).
[25] H. Itoh, M. Yoshikawa, I. Nashiyama, S. Misawa, H. Okumura, and S. Yoshida, IEEE Trans. Nucl. Sci. **37**, 1732 (1990).
[26] H. Itoh, M. Yoshikawa, L. Wei, S. Tanigawa, I. Nashiyama, S. Misawa, H. Okumura, and S. Yoshida, Mater. Res. Soc. Symp. Proc. **262**, 331 (1992).
[27] H. Itoh, M. Yoshikawa, I. Nashiyama, S. Misawa, H. Okumura, and S. Yoshida, J. Electronic Mater. **21**, 707 (1992).
[28] H. Itoh, M. Yoshikawa, I. Nashiyama, S. Misawa, H. Okumura, and S. Yoshida, Inst. Phys. Conf. Ser. No. 137, 255 (1994).
[29] H. Itoh, M. Yoshikawa, I. Nashiyama, L. Wei, S. Tanigawa, S. Misawa, H. Okumura, and S. Yoshida, Mater. Sci. Forum **117/118**, 501 (1993).
[30] H. Itoh, M. Yoshikawa, I. Nashiyama, L. Wei, S. Tanigawa, S. Misawa, H. Okumura, and S. Yoshida, Hyperfine Interactions **79**, 725 (1993).
[31] H. Itoh, M. Yoshikawa, I. Nashiyama, H. Okumura, S. Misawa, and S. Yoshida, J. Appl. Phys. **77**, 837 (1995).
[32] N. T. Son, E. Sörman, W. M. Chen, M. Singh, C. Hallin, O. Kordina, B. Monemar, E. Janzén, and J. L. Lindström, J. Appl. Phys. **79**, 3784 (1996).

[33] G. D. Watkins and J. W. Corbett, Phys. Rev. **134**, A1359 (1964).
[34] P. A. Kumar, K. G. Lynn, and D. O. Welch, J. Appl. Phys. **76**, 4935 (1994).
[35] P. Kirkegaard, N. Pederson, and M. Eldrup, PATFIT-88, Riso-M-2704, 1989.
[36] H. Itoh, M. Yoshikawa, I. Nashiyama, S. Misawa, H. Okumura, and S. Yoshida, in: Amorphous and Crystalline Silicon Carbide III, Eds. G. L. Harris, M. G. Spencer, and C. Y. Yang, Springer-Verlag, Berlin 1992 (p. 143).
[37] J. Isoya, H. Kanda, Y. Uchida, S. C. Lawsonn, S. Yamasaki, H. Itoh, and Y. Morita, Phys. Rev. B **45**, 1436 (1992).
[38] B. A. Goodman and J. B. Raynor, in: Advances in Inorganic Chemistry and Radiochemistry Vol. 13, Eds. H. J. Emeleus and A. G. Sharpe, Academic Press, New York 1970 (p. 135).
[39] J. W. Corbett and G. D. Watkins, Phys. Rev. **138**, A555 (1965).
[40] J. A. van Vechten, in: Handbook of Semiconductors, Vol. 3, Material Properties and Preparation, Eds. T. S. Moss and S. P. Keller, North-Holland Publ. Co., Amsterdam, 1980.
[41] A. Uedono, H. Itoh, T. Ohshima, Y. Aoki, M. Yoshikawa, I. Nashiyama, H. Okumura, S. Yoshida, T. Moriya, T. Kawano, and S. Tanogawa, Japan. J. Appl. Phys. **35**, 5986 (1996).
[42] A. Uedono, T. Kitano, M. Watanabe, T. Moriya, T. Kawano, S. Tanigawa, R. Suzuki, T. Ohdaira, and T. Mikado, Japan. J. Appl. Phys. **35**, 2000 (1996).
[43] J.-L. Lee, A. Uedono, S. Tanigawa, and J. Y. Lee. J. Appl. Phys. **67**, 6153 (1990).
[44] S. Dannefaer, B. Hogg, and D. Kerr, Phys. Rev. B **30**, 3355 (1984).
[45] S. Dannefaer, D. Craigen, and D. Kerr, Phys. Rev. B **51**, 1928 (1995).
[46] J. Keinonen, M. Hautala, E. Rauhala, V. Karttunen, A. Kuronen, J. Räisänen, J. Lahtinen, A. Vehanen, E. Punkka, and P. Hautojärvi, Phys. Rev. B **37**, 8269 (1988).
[47] A. Uedono, S. Tanigawa, J. Sugiura, and M. Ogasawara, Japan. J. Appl. Phys. **29**, 1867 (1990).
[48] A. Uedono, L. Wei, C. Dosho, H. Kondo, S. Tanigawa, J. Sugiura, and M. Ogasawara, Japan. J. Appl. Phys. **30**, 201 (1991).
[49] A. Kawasuso, H. Itoh, S. Okada, and H. Okumura, J. Appl. Phys. **80**, 5639 (1996).
[50] G. Brauer, W. Anwand, E.-M. Nicht, J. Kuriplach, M. Sob, N. Wagner, P. G. Coleman, M. J. Puska, and T. Korhonen, Phys. Rev. B **54**, 2512 (1996).
[51] G. Brauer, W. Anwand, P. G. Coleman, A. P. Knights, F. Plazaola, Y. Pacaud, W. Skorupa, J. Störmer, and P. Willutzki, Phys. Rev. B **54**, 3084 (1996).
[52] R. Babcock, IEEE Trans. Nuclear Sci. **12**, 43 (1965).
[53] A. Kawasuso, H. Itoh, T. Ohshima, N. Morishita, D. Cha, M. Yoshikawa, I. Nashiyama, S. Okada, H. Okumura, and S. Yoshida, unpublished.
[54] W. J. Choyke, Z. C. Feng, and J. A. Powell, J. Appl. Phys. **64**, 3163 (1988).
[55] H. Okumura, M. Shinohara, S. Kuroda, K. Endo, E. Sakuma, S. Misawa, and S. Yoshida, Japan. J. Appl. Phys. **27**, 1712 (1988).
[56] V. S. Vainer and V. A. Ilin, Soviet Phys. – Solid State **23**, 1432 (1981).
[57] D. S. Nedzvetskii, B. V. Novikov, N. K. Prokofeva, and M. B. Teitman, Soviet Phys. – Semicond. **2**, 914 (1968).